Sadegh Pour-Ali[a], Ali-Reza Kiani-Rashid[a], Abolfazl Babakhani[a], Sannakaisa Virtanen[b]

[a] Materials and Metallurgical Engineering Department, Faculty of Engineering, Ferdowsi University of Mashhad, Mashhad, Iran
[b] Department of Materials Science, WW4-LKO, University of Erlangen-Nuremberg, Erlangen, Germany

Severe shot peening of AISI 321 with 1000 % and 1300 % coverages: A comparative study on the surface nanocrystallization, phase transformation, sub-surface microcracks, and microhardness

In this study, AISI 321 austenitic stainless steel samples were surface treated using severe shot peening (SSP) with 1000 % and 1300 % coverages. Microstructural features including the grain size, phase transformation, and formation of sub-surface microcracks were investigated at the rough top surface and about 40 μm depth (top surface after grinding and removal of initial rough surface layer created by SSP). In addition, microhardness variations were thoroughly analyzed in-depth. Experimental results demonstrated that for both 1000 % and 1300 % coverages, the microstructures of top surface and 40 μm depth are respectively composed of equiaxed nano-grains and lamella-shaped cells; however, enhanced imparted strain in the case of 1300 % coverage leads to the formation of considerable amounts of strain-induced martensite (α') phase in the surface layers and consequently, due to strength increase and lack of deformability, some microcracks are created in the sub-surface layers (up to 20 μm depth).

Keywords: 321 stainless steel; Severe shot peening; Surface nanocrystallization; Microhardness; Sub-surface microcracks

1. Introduction

Higher hardness and strength, improved fatigue behavior, enhanced electrical resistivity, higher thermal expansion coefficient, improved corrosion and tribological properties, better low temperature plasticity and higher adsorption capacity are the main properties that distinguish nanocrystalline (NC) materials from their coarse-grained counterparts [1–5]. There are different techniques to develop bulk NC materials including severe plastic deformation (SPD) [6], chemical vapor deposition (CVD) and physical vapor deposition (PVD) [7], crystallization of amorphous precursors [8], ball milling [9], electrodeposition [10], etc.; however, development of an ideal bulk NC material (free of porosity and contamination, bulk in size, uniform and ultrafine in grain size) is still a challenge in materials science [11]. It is well known that most material failures are initiated from the topmost surface and completely dependent on the properties and structure of the material surface [12]. So, in many cases, surface modification can serve as an effective way to prevent and/or postpone material failure. In this way, surface nanocrystallization (SNC) as a renowned surface modification method has attracted considerable attention in both academia and industry. Severe shot peening (SSP) [13, 14], surface mechanical attrition treatment (SMAT) [15, 16], cold rolling [17], ultrasonic impact peening [18, 19], severe wire brushing [20], high-speed drilling [21], and laser shock peening (LSP) [22] are among the most applicable processes for the SNC of different metallic materials. In these techniques, large plastic strains with high strain rates are imparted to initial coarse grains in order to create a large number of crystallographic defects (vacancies, dislocations, grain boundaries, etc.) and consequently refine the grains.

Among the mentioned techniques for SNC, SSP is a common surface treatment in industry, which enables the formation of nanocrystalline layers on the surface of bulk metallic materials and improves their applicability. Bagherifard et al. [23] produced a nanocrystalline surface layer on cast iron via SSP and reported that this layer can improve the fatigue strength and crack initiation resistance. Raja et al. [24] reported that the nanocrystalline surface layer in an Ni–Cr–Mo–W alloy fabricated through SSP leads to superior corrosion resistance and claimed that this improvement is attributed to the better electronic properties in the presence of dense grain boundaries and dislocations. Ma et al. [25] reported that the tribological properties of 1Cr18Ni9Ti stainless steel were greatly enhanced after SNC by the SSP. They pointed out that this enhancement is directly related to change in wear mechanism of original 1Cr18Ni9Ti stainless steel from abrasive/adhesive wear to fatigue wear. Hassani-Gangaraj et al. [26] studied the effect of coverage of SSP on the SNC and the ultrafine-graining of sub-surface layers of a low alloy steel and developed a model linking finite element simulation of SSP to dislocation density evolution. These researchers used severe shot

Int. J. Mater. Res. (formerly Z. Metallkd.) 109 (2018) 5

451

peening (more than 1 000 % coverage) to refine the initial grains.

The mentioned reports have focused on the beneficial effect of SSP, i.e. nanocrystallization/ultrafine-graining in the surface layers and were less concerned about the side effects of SSP. According to the nature of the SSP process (imparting high energy and creating some crystallographic defects in the initial grains), this issue should be more considered in that using the SSP may introduce some side effects including the formation of sub-surface microcracks, phase transformation(s), enhancement of the surface brittleness, a considerable change in the surface roughness, etc. Such changes are not negligible because they can significantly influence all the benefits of grain refinement. Actually, a thick nanocrystalline surface layer on the bulk metallic materials with a small surface roughness and without any microcrack is the ideal state after SSP. Hence, having a proper understanding of the side effects of SSP will be helpful in the performance of treated parts for subsequent applications. In this paper, two SSP processes with 1 000 % and 1 300 % coverages were used to fabricate a gradient nanocrystalline structure on the surface of 321 stainless steel (321SS) alloy. The reason for choosing 1 000 % and 1 300 % coverages was that these levels of coverage have been successfully used to create an integration of ultrafine-/nano-grains on the surface of Fe-based alloys [13, 14, 26 – 33]; however, the mentioned side effects of SSP have not been experimentally studied for these coverages. According to the surface roughness values, in order to get a smooth surface after SSP, it was necessary to grind the shot peened samples up to 40 µm depth. So, the topmost surface and ≈ 40 µm depth (topmost surface after grinding) of the treated samples were analyzed by grazing incidence X-ray diffraction (GI-XRD), field-emission scanning electron microscopy (FE-SEM) and transmission electron microscopy (TEM). In line with the grain refinement examination, side effects of the SSP including the phase transformation, surface roughness, sub-surface microcrack formation, and microhardness variations were also comparatively investigated.

2. Experimental procedure

The material used in the present study was a hot rolled/cold finished 321SS alloy bar (STOOSS Co., Switzerland) with a diameter of 80 mm and the following chemical composition (wt.%): 0.021 C, 0.557 Si, 1.485 Mn, 18.104 Cr, 0.113 Mo, 9.697 Ni, 0.016 P, 0.011 S, 0.461 Ti and balance Fe. In order to get a homogeneous chemical composition, the bar was solution annealed at 1 100 °C for 2 h and after that quenched in water. Cylindrical specimens of 6.0 mm thickness were sectioned from the bar, ground (up to 1 200 grit), polished (up to 1 µm) and subjected to SSP using an air blast apparatus (KPS SHOT Co.). For the SSP, standard high carbon steel shot (S230) with a nominal diameter of 0.58 mm and hardness of 45 – 50 HRC were used. The SSP process was carried out by a peening nozzle (diameter of 30 mm), mass flow rate of about 8 kg min^{-1}, and air pressure of 45 psi with 1 000 % and 1 300 % coverages. To generate reproducible plastic strains, the shot angle and the distance between the nozzle and top surface were set to 90° and 400 mm, respectively.

The cross-sections of shot peened samples for SEM observations were mechanically ground, polished and afterward etched in a solution containing 2.5 ml H$_2$O, 2.5 ml HNO$_3$ and 5 ml HCl. SEM images were taken on a TESCAN MIRA3 field emission scanning microscope at 15 kV. The GI-XRD studies were carried out using an X'Pert Pro MPD X-ray diffraction instrument operated with Cu-K$_\alpha$ radiation and grazing angle of 2°. Average grain size in the surface and different depths was estimated according to the Williamson–Hall equation [34, 35]:

$$\beta_{\mathrm{r}} \cos \theta = \left(\frac{k\lambda}{D} \right) + \mu \sin \theta \qquad (1)$$

where D is the grain size, k is the Scherrer factor which is usually 0.9, μ is representative of strain, λ and θ are the wavelength of the irradiated X-ray wavelength and Bragg's angle, respectively. The β_{r} in Eq. (1) is equal to peak broadening of diffraction peaks due to the SSP. In fact, β_{r} is equal to $\sqrt{\beta_{\mathrm{i}}^2 - \beta_0^2}$, in which β_{i} and β_0 are full widths at half maximum (FWHM) of diffraction peaks of shot peened and non-treated sides of 321SS samples, respectively. The volume fraction of martensite phases was also determined by Rietveld refinement using the GSAS software [36]. Grain refinement of the treated samples was also characterized by transmission electron microscopy (TEM) and selected area electron diffraction (SAED) methods (Tecnai G2 operating at 200 kV). To validate the grain size values obtained from XRD measurements, this parameter was also statistically determined through dark-field TEM imaging. GI-XRD and TEM analyses at the topmost surface were done similar to [26]. For the GI-XRD examination at ≈ 40 µm depth, shot peened 321SS samples were wet microground/polished from the treated surface to reach this depth and then the GI-XRD test was run. After that, these samples were ground and polished from the untreated surface to get an overall thickness of about 50 µm, afterward prepared foils were perforated by dimpling and ion-milled for the TEM microscopy at ≈ 40 µm depth. The thickness of samples was regularly measured by a screw thread micrometer. For each position (topmost surface and ≈ 40 µm depth), five specimens were considered to study the corresponding microstructure. In-depth microhardness measurements were made on a Buehler microhardness tester at a load of 20 g and dwell time of 10 s. In addition, a non-contact optical profilometer (NewView$^{\mathrm{TM}}$ 8000 3D optical surface profiler, Zygo Corporation, Ohio) was used to measure the surface roughness of different samples.

3. Results and discussion

3.1. The microstructure prior to SSP

Figure 1 shows the microstructural characteristics of 321SS alloy prior to the SSP. Considering the chemical composition of 321SS alloy, especially Ni and Mn contents (austenite stabilizer elements) and its XRD pattern (Fig. 1c), the microstructure consists of γ grains (austenite) as the matrix and martensite phase as fine needles inside of the γ grains. According to the Rietveld refinement, the $V_{\mathrm{martensite}}$ value is about 10 % which in turn shows that the austenite is the main phase in the solution annealed state of 321SS alloy.
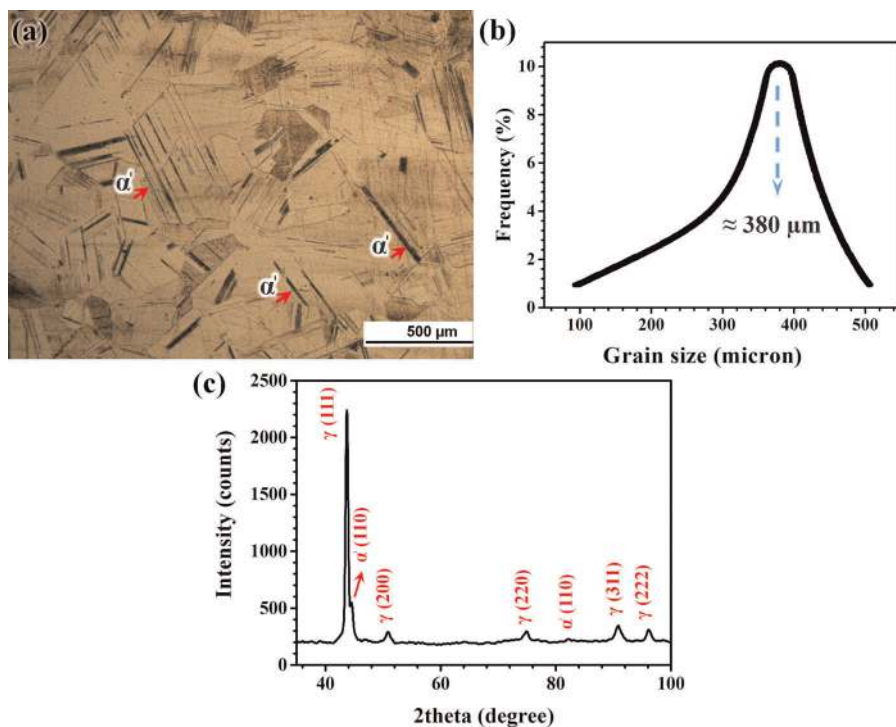
Fig. 1. (a) The original microstructure of 321SS alloy before SSP, (b) the γ grain size distribution, and (c) corresponding XRD pattern.
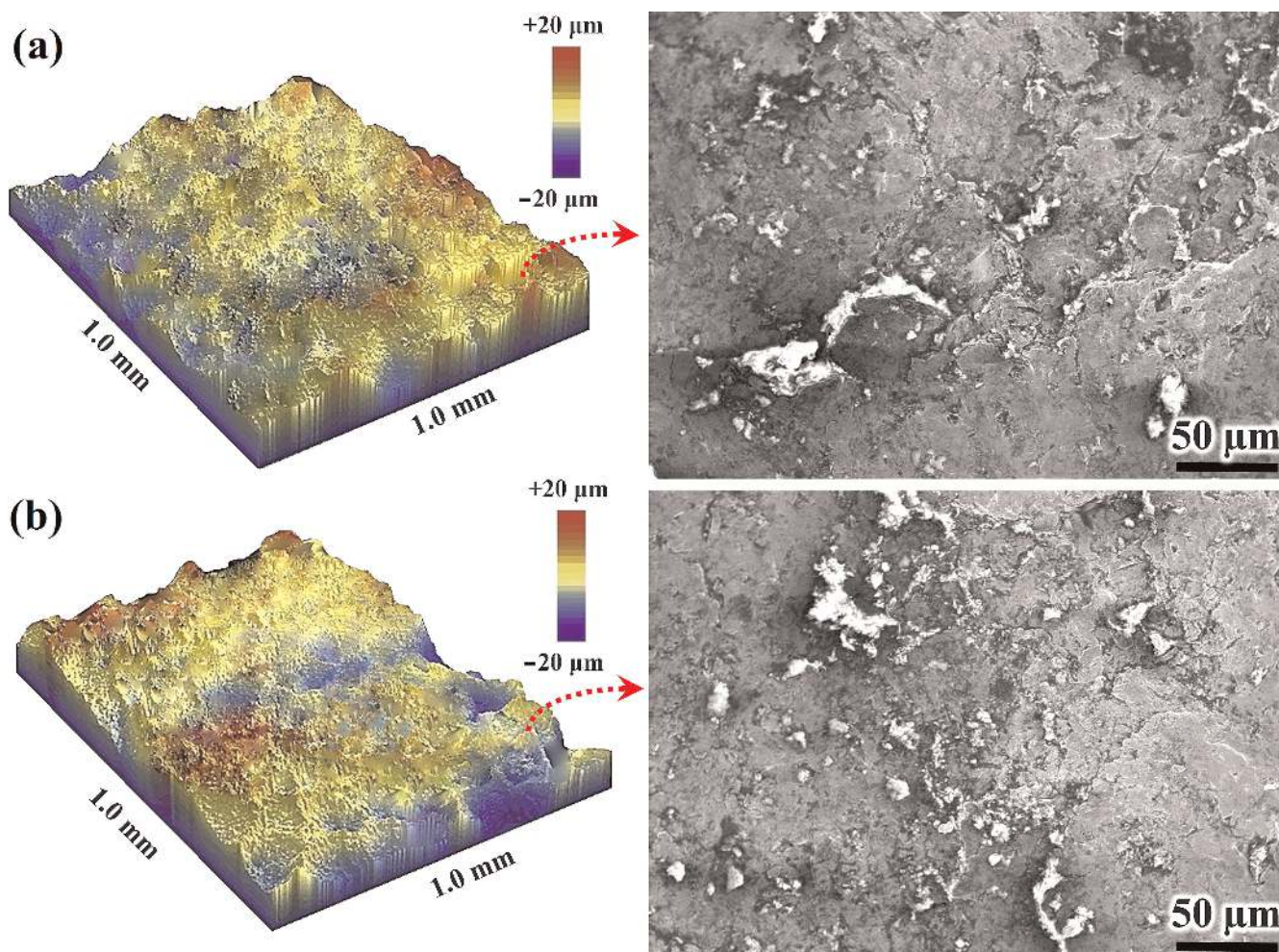
Fig. 2. Three dimensional surface roughness and surface appearance (SEM images) of severely shot peened samples: (a) 1 000 %, and (b) 1 300 % coverages.

The grain size distribution of primary γ phase measured by microstructural image processing (MIP) software is shown in Fig. 1b. It can be seen that the average grain size of primary γ phase is comparable with the annealed state of 321 SS (about 380 μm).

3.2. Surface roughness

Figure 2 and Table 1 show the surface roughness profiles/ surface morphology and surface roughness values, respectively. All values are based on the definition of ISO 4287 [37]. The arithmetic-mean (R_a) is oftenly considered as the representative parameter of surface roughness; however, largest peak to valley height (R_t) is more important in the case of shot peened surfaces. This is due to the necessity of grinding of these surfaces and removal of a surface layer as thick as R_t after the SSP to get a smooth surface. As can be seen from SEM images in Fig. 2, the appearance of rough surfaces generated by both 1 000 % and 1 300 % coverages are quite similar. Both surfaces show evidence of a flaky surface with overlaps and microscaling. The borders of some overlaps have a white color which indicates that the surfaces of both samples have been strongly plasticized [31]. Surface roughness parameters (R_a, R_q, and R_t) are also comparable (Table 1). Although some researchers have stated that the surface roughness increases as the coverage increases [38], for the high coverages due to enhanced work hardening in the surface layers, surface roughness profile shows nearly stable values. As numerically modeled by Labeas et al. [32], there are three stages in the surface roughness evolution. In the first stage (low coverages), some areas are not covered and the peak-to-valley roughness (R_t) has the highest possible value. In the second stage (middle coverages), more areas are covered and the sharp lips formed in the first stage become smoother. Finally, in the third stage, the surface roughness decreases and comes to a stable profile (similar to Fig. 2). This profile is mainly dependent on the material and shot peening parameters [39, 40].

3.3. XRD analysis

XRD patterns of the shot peened samples at the topmost surface and 40 μm depth are shown in Fig. 3. Comparing these patterns with Fig. 1c reveals significant changes in the volume fractions of phases and full width at half maximum (FWHM) of different peaks. As can be seen from Fig. 3, the intensity of α′ peaks remarkably increases for the surface of both 1 000 % and 1 300 % coverages; however, this increment is more obvious in the latter case. Based on the Rietveld refinement, the $V_{\alpha'}$ (α′: strain induced martensite) value at the surface of shot peened 321SS is increased to 80 % and 65 % for 1 300 % and 1 000 % cov-

erages, respectively. With increasing depth, the imparted plastic stain is dramatically decreased [26] and consequently, $V_{\alpha'}$ values are also decreased. So, this value drops to 43 % (1 300 % coverage) and 38 % (1 000 % coverage) for 40 μm depth. In addition to the phase evolution, comparing with the XRD pattern of annealed 321SS (Fig. 1c), a considerable broadening in diffraction peaks of these surface layers is observed. According to Eq. (1), this broaden-
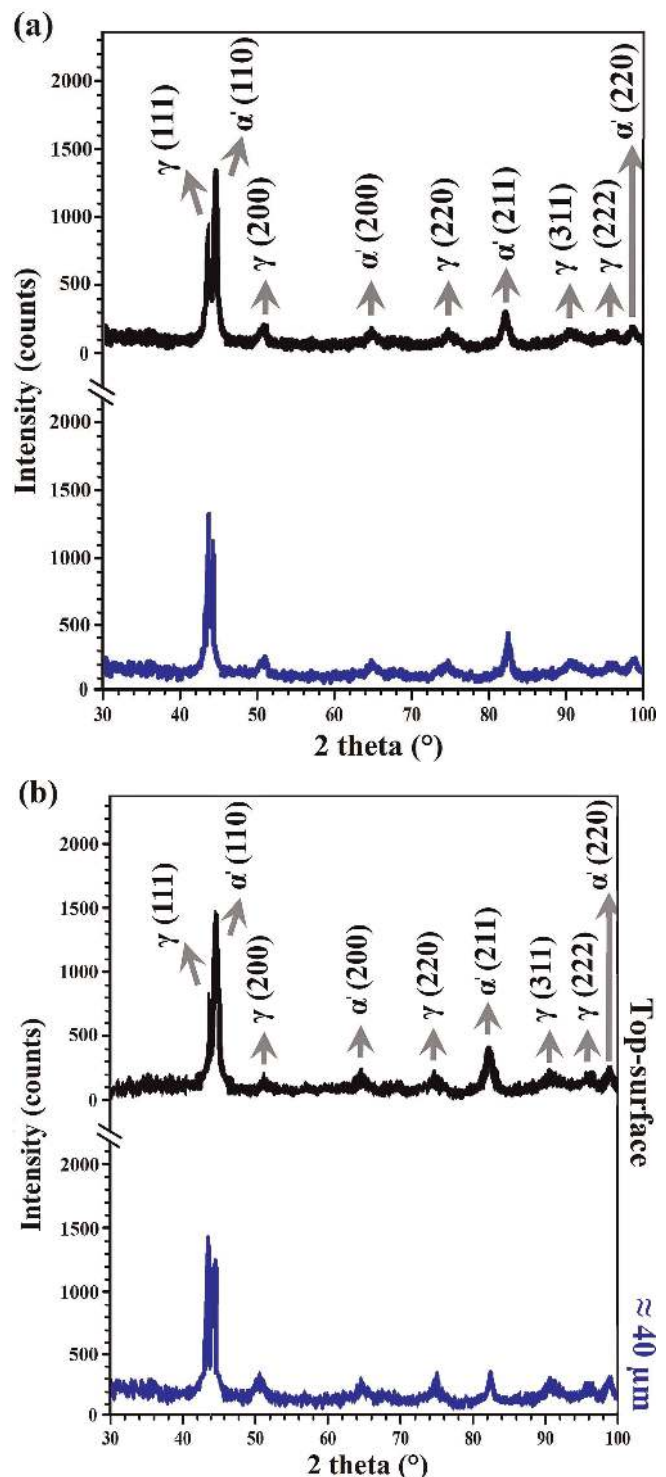
Fig. 3. XRD patterns from the surface and ≈ 40 μm below the rough top surfaces of shot peened samples with (a) 1 000 %, and (b) 1 300 % coverages.

Table 1. Surface roughness parameters of the severely shot peened 321SS samples.

Sample	R_a (μm)	R_q (μm)	R_t (μm)
1 000 % coverage	13.3 ± 3.5	20.9 ± 7.2	31.5 ± 5.2
1 300 % coverage	16.4 ± 2.6	19.3 ± 5.4	32.8 ± 4.8

ing is mostly attributed to the grain refinement and an increase in the microstrain. The results of the Williamson–Hall analysis of the top surface and 40 μm below the top surface of treated samples are presented in Fig. 4. In this way, the average surface grain size of the 321SS samples shot peened with 1300 and 1000% coverages are 48.6 and 53.5 nm, respectively. These values increased to 87.2 nm (1300% coverage) and 93.6 nm (1000% coverage) for 40 μm depth. Thus, based on XRD analysis, it can be claimed that the $\gamma \rightarrow \alpha'$ phase transformation in the surface and 40 μm depth of 321SS alloy will be severely affected by increasing the SSP coverage from 1000% to 1300%. In addition, these results clearly verify that the grain size at the top surface and 40 μm depth in 1000% coverage are correspondingly comparable with the 1300% coverage.

3.4. SEM and TEM analyses

Figure 5 displays typical SEM images from the cross-section of severely shot peened 321SS samples. As can be
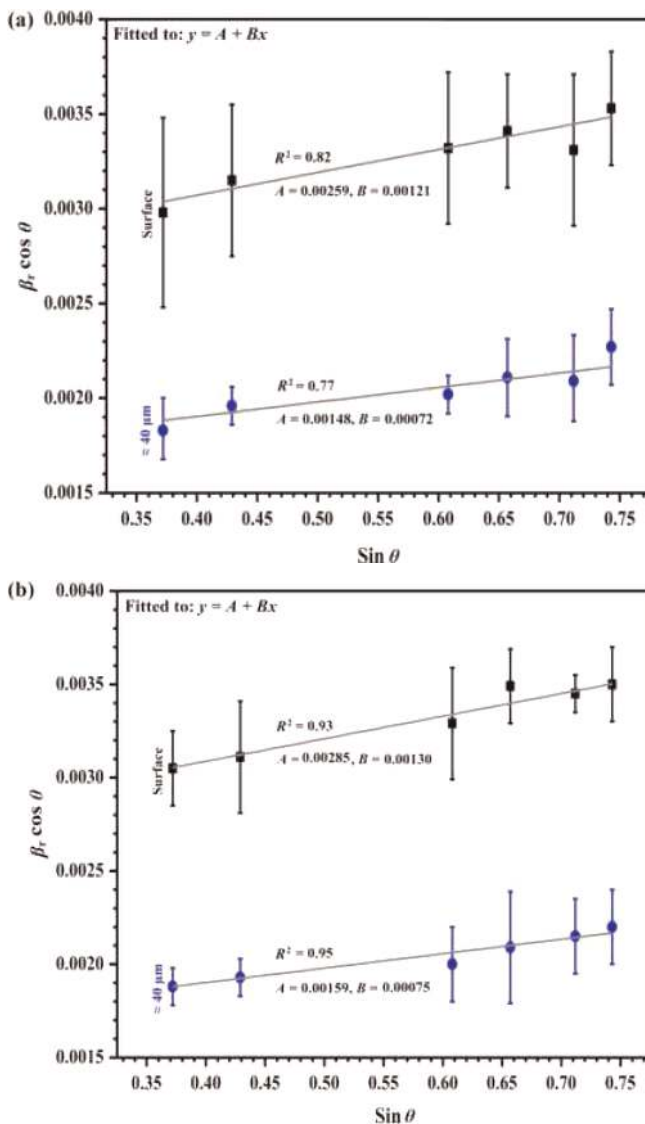
Fig. 4. Williamson–Hall analyses from the surface and 40 μm depth of severely shot peened samples with (a) 1000%, and (b) 1300% coverages.

seen, microstructural differences between the deformation affected zone and the matrix are distinct; however, there is not a sharp boundary between them. The total thickness of the deformation affected layer is about 120 μm which is much bigger than that of reported for LSP [22] and SMAT [15] of austenitic stainless steels. Based on the high magnification images taken from the top surface layers of treated samples (Fig. 5b, c, e, and f), severe microcracking is the main microstructural feature for the 1300% coverage (up to 20 μm below the rough top surface). Regardless of the surface nanocrystallization, these microcracks can be considered as favorable sites for stress concentration and crack nucleation. In this way, they can remarkably compromise the mechanical and tribological properties [41]. In the case of 1000% coverage, similar morphology without microcracking is observed. In fact, high coverages of the SSP (e.g. 1300%) lead to greater work hardening and consequently microcracking in the surface layers. Figure 6 shows bright field TEM micrographs and corresponding SAED patterns of the microstructure of the top surface and ≈ 40 μm below the top surface of treated samples. A nearly full surface nanocrystallization is obtained in both 1000% and 1300% coverages, so that extremely fine and equiaxed nano-grains with random crystallographic orientation and size of 70–75 nm are observed in the whole microstructure. This value is larger than the XRD result. In fact, the crystallite size obtained by XRD analysis is defined as the size of the coherent scattering domains, consequently XRD can distinguish the subgrains with small misorientations and give the average size of subgrains. However, conventional TEM imaging provides the average size of the grains with higher angle grain boundaries. This microstructural refinement is also reflected in the SAED patterns, where continuous rings (1000%) appear instead of streak points. Considering the lattice parameters ($a_\gamma = 3.575$ A°, $a_{\alpha'} = 2.868$ A°), observed diffraction rings can be directly assigned to both γ and α' phases (see Fig. 6). Similar observations have also been reported for comparable surface treatments [42]. In the case of 40 μm depth (Fig. 6b and d), the main microstructural feature is the formation of lamella-shaped cells. As is obvious from Fig. 6b and d, the boundaries of these cells are not as straight as those of the mechanical twins and many dislocation pile-ups are observed in these boundaries. The corresponding SAED patterns (imperfect rings) also exhibit microstructural evolution and transition to coarser grains compared with the nano-grains on the rough top surfaces. Thus, it can be claimed that both the 1000% and 1300% coverages show comparable grain structure at the rough top surface and 40 μm depth.

3.5. In-depth microhardness variations

Microhardness variation with the depth from 10 μm below the topmost surface towards the matrix of severely shot peened samples is shown in Fig. 7. The value of each data point is the arithmetic mean of at least three single indentations at the same depth, and the error bars show the mean standard deviations. As can be seen, the top surface of the sample with 1300% coverage possesses the highest microhardness (≈ 316 HV) and with moving away from the top surface this parameter is gradually decreased and finally reaches the matrix hardness. Although a similar trend is observed for the 1000% coverage, the highest microhardness
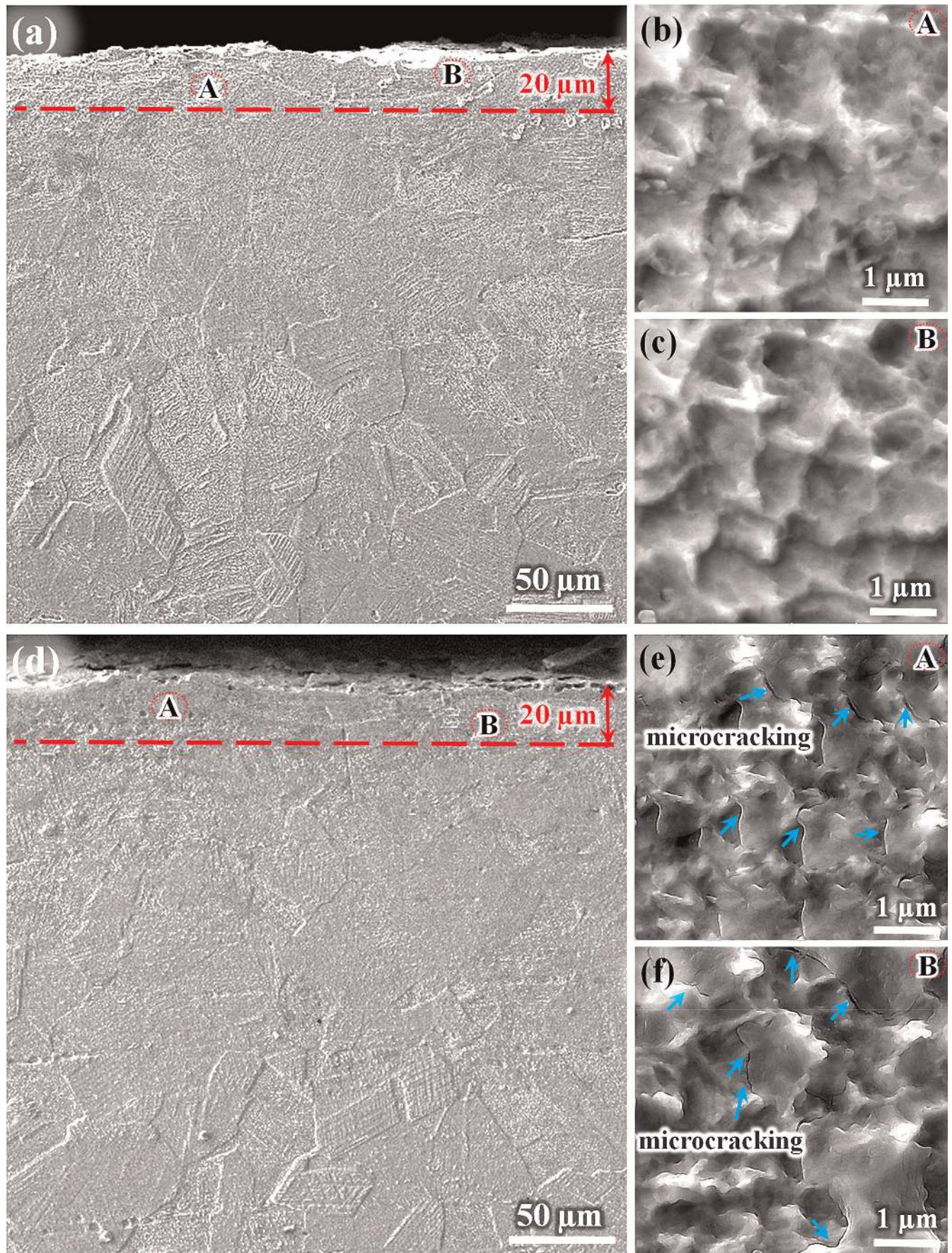
Fig. 5. Cross-sectional SEM images of the severely shot peened samples with (a, b and c) 1000 %, and (d, e and f) 1300 % coverages.

is around 35 HV less than 1300 % one. Microhardness increase in the surface layers after SSP is mainly due to the following reasons:

1. In the terms of the Hall–Petch relationship [43], a larger reduction in the grain size is reflected in an increase in the hardness.
2. The presence of excessive amounts of α′ phase in the surface layers of treated samples can reinforce the γ matrix and consequently increase the microhardness of the whole microstructure. This statement is in good agreement with the reports by Mordyuk et al. [44, 45].

Both TEM and XRD results showed that the grain size at the rough top surface and 40 μm depth are comparable in both 1000 and 1300 % coverages. Thus, higher microhardness in the surface layers of the treated sample with 1300 % coverage is directly related to the formation of more α′ phase which in turn can increase the microhardness of 321SS alloy.

Many researchers have focused on the mechanism of nanocrystallization and ultrafine-graining after SSP [24–27, 46]; however, the mechanism of microcrack formation during SSP was not investigated in detail. Figure 8 shows a physical mechanism for the formation of microcracks. SSP can be divided into three steps in total: (1) Plastic deformation is introduced to surface layers; (2) In order to minimize the total energy of the system, surface grains are gradiently refined and reduced to nano-size (topmost surface); (3) Microcracks form in the nano-layer under over processing. For

321SS, the stacking fault energy (*SFE*) is about 78 mJ m^{-2} [47] and both dislocation slipping and formation of microtwins with nanometer-sized are responsible for deformation. With increasing SSP coverage to more than 1000 %, the surface layer is processed into nano-grains and its strength is sharply increased. At the same time, $V_{\alpha'}$ values
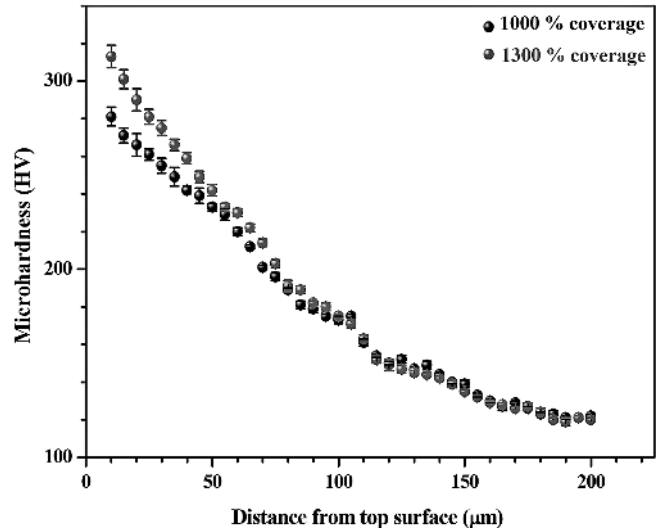
Fig. 7. Variation of microhardness with depth in the severely shot peened 321SS samples.
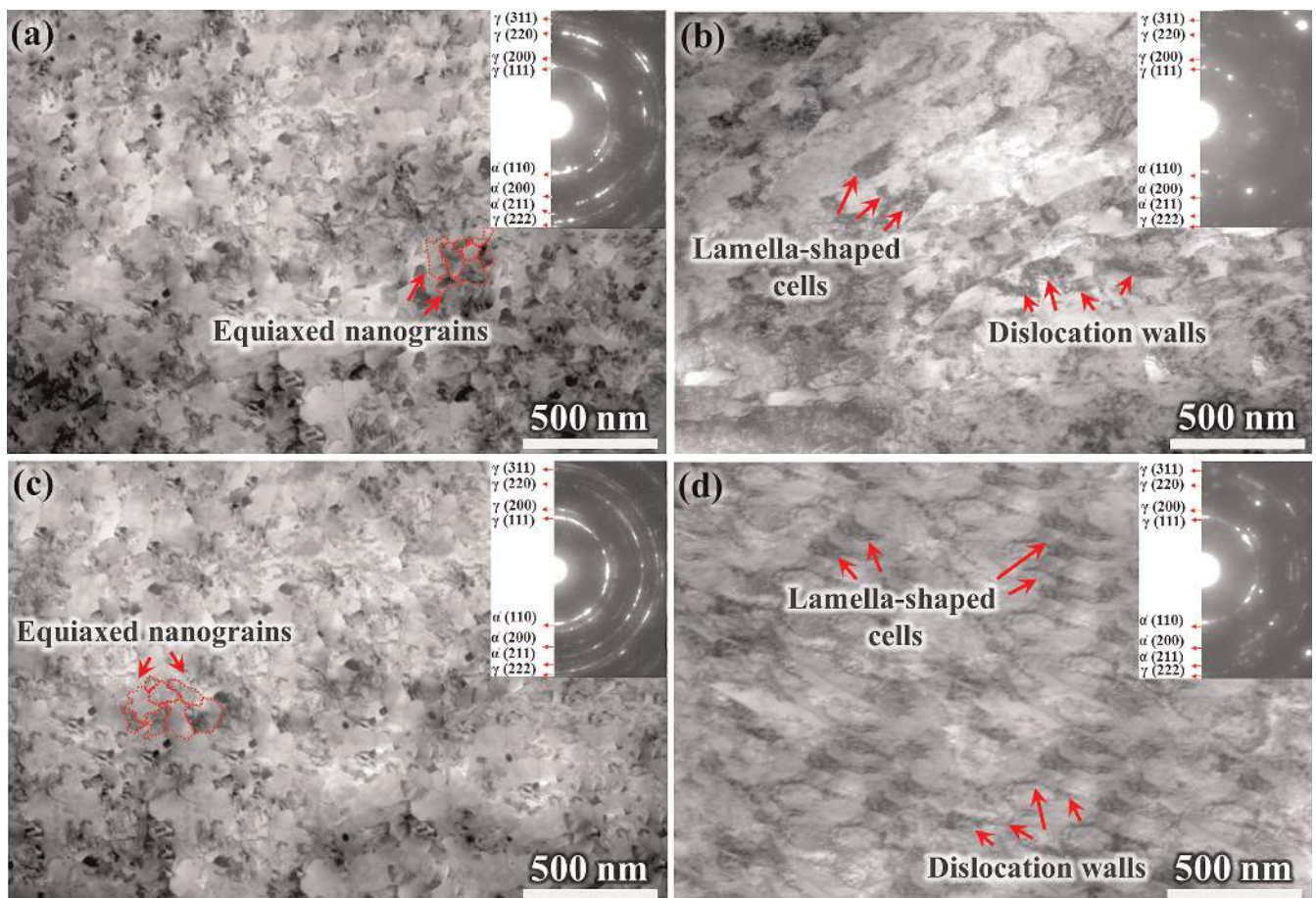
Fig. 6. Bright field TEM micrographs and corresponding SAED patterns taken from the (a and c) topmost surface, and (b and d) ≈ 40 μm depth of the shot peened samples with (a and b) 1000 %, and (c and d) 1300 % coverages.
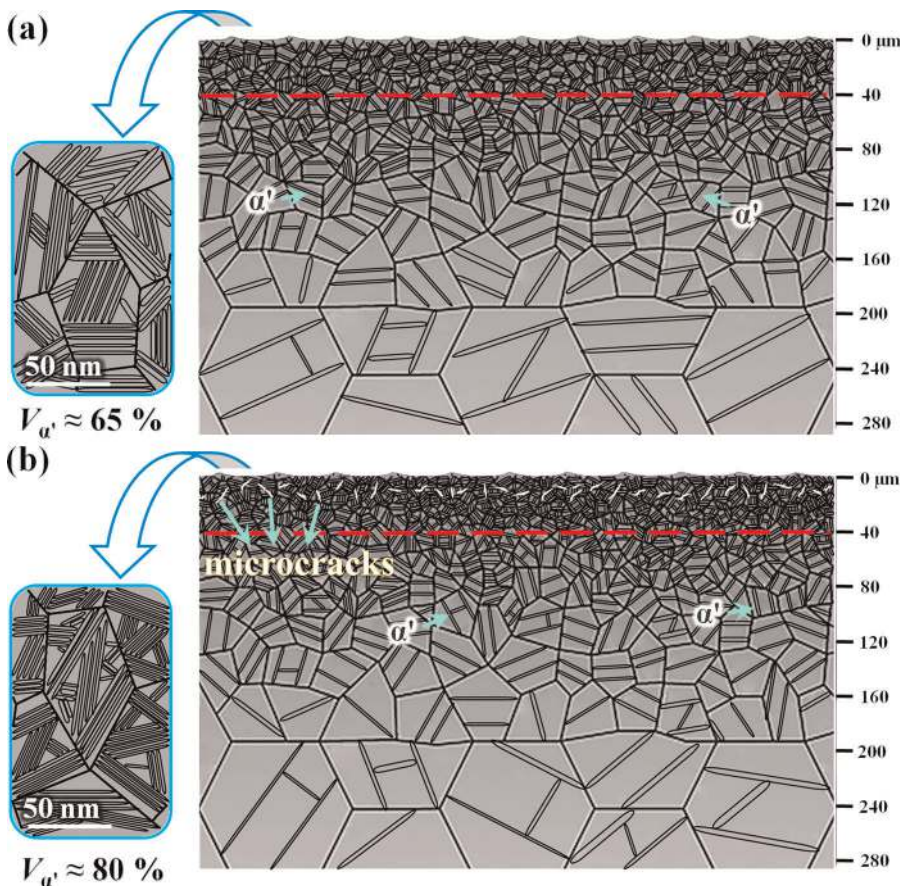
Fig. 8. The evolutionary process of the microstructure of surface layers of 321SS during SSP with: (a) 1 000 %, and (b) 1 300 % coverages.

are also increased. In this way, top surface layers are characterized by nano-sized grains and α′ phase, both of which induce high strength but decrease deformability. A high energy shot peening such as 1 300 % coverage, not only refines the grains in the surface layers but also promotes the brittleness of nano-grained layer and produces some microcracks in the top surface layers (Figs. 5e, f and 8).

4. Conclusions

On the basis of the results, the following conclusions can be drawn:

1. Both 1 000 % and 1 300 % coverages are successful in the formation of a nanocrystalline layer on the rough top surface of 321SS alloy.
2. Formation of lamella-shaped cells at ≈ 40 μm below the top surface is the common microstructural feature for both 1 000 % and 1 300 % coverages.
3. $V_{α'}$ values for the top surface layer of 321SS treated with 1 000 % and 1 300 % coverages are increased by 65 % and 80 %, respectively.
4. In the case of both 1 000 % and 1 300 % coverages, due to enhanced work hardening in the surface layers, surface roughness profiles show nearly stable values (R_t fluctuates between 26.3 and 37.6 μm).
5. Formation of a high strength layer with lack of deformability on the surface of 321SS after SSP with 1 300 % coverage induced microcracks in the nano-grained subsurface layer.

References

[1] M.A. Meyers, A. Mishra, D.J. Benson: Prog. Mater. Sci. 51 (2006) 427–556. DOI:10.1016/j.pmatsci.2005.08.003
[2] C. Gu, J. Lian, J. He, Z. Jiang, Q. Jiang: Surf. Coat. Technol. 200 (2006) 5413–5418. DOI:10.1016/j.surfcoat.2005.07.001
[3] Y.S. Zhang, Z. Han, K. Wang, K. Lu: Wear. 260 (2006) 942–948. DOI:10.1016/j.wear.2005.06.010
[4] L. Wang, J. Li, Y. Wang, L. Zhao, Q. Jiang: Chem. Eng. J. 181–182 (2012) 72–79. DOI:10.1016/j.cej.2011.10.088
[5] C. Suryanarayana: Bull. Mater. Sci. 17 (1994) 307–346. DOI:10.1007/BF02745220
[6] Y. Wang, X. Liao, Y. Zhu: Int. J. Mater. Res. 100 (2009) 1632–1637. DOI:10.3139/146.110230
[7] M.T. Swihart: Curr. Opin. Colloid Interface Sci. 8 (2003) 127–133. DOI:10.1016/S1359-0294(03)00007-4
[8] M.L. Trudeau: Nanophase Mater. Synth. Prop. Appl., Springer Netherlands, Dordrecht, 1994: pp. 153–156. DOI:10.1007/978-94-011-1076-1_21
[9] M. Hafezi, A. Nadernezhad, M. Mohammadi, H. Barzegar, H. Mohammadi: Int. J. Mater. Res. 105 (2014) 469–473. DOI:10.3139/146.111048
[10] Q. Li, H. Lu, J. Cui, M. An, D. Li: Surf. Coat. Technol. 304 (2016) 567–573. DOI:10.1016/j.surfcoat.2016.07.056
[11] B. Altan: Severe plastic deformation: toward bulk production of nanostructured materials, Nova Publishers, 2006.
[12] S. Pour-Ali, A. Kiani-Rashid, A. Babakhani: Int. J. Mater. Res. 107 (2016) 1031–1040. DOI:10.3139/146.111432

458

Int. J. Mater. Res. (formerly Z. Metallkd.) 109 (2018) 5

[13] S. Pour-Ali, A.-R. Kiani-Rashid, A. Babakhani: Vacuum. 144 (2017) 152–159. DOI:10.1016/j.vacuum.2017.07.016

[14] S. Pour-Ali, A.-R. Kiani-Rashid, A. Babakhani, S. Virtanen: Vacuum. 146 (2017). 297–303. DOI:10.1016/j.vacuum.2017.09.053

[15] T. Roland, D. Retraint, K. Lu, J. Lu: Scr. Mater. 54 (2006) 1949–1954. DOI:10.1016/j.scriptamat.2006.01.049

[16] A.L. Ortiz, J.-W. Tian, L.L. Shaw, P.K. Liaw: Scr. Mater. 62 (2010) 129–132. DOI:10.1016/j.scriptamat.2009.10.015

[17] V. Demers, V. Brailovski, S.D. Prokoshkin, K.E. Inaekyan: J. Mater. Process. Technol. 209 (2009) 3096–3105. DOI:10.1016/j.jmatprotec.2008.07.016

[18] B.N. Mordyuk, O.P. Karasevskaya, G.I. Prokopenko, N.I. Khripta: Surf. Coat. Technol. 210 (2012) 54–61. DOI:10.1016/j.surfcoat.2012.08.063

[19] B.N. Mordyuk, G.I. Prokopenko, M.A. Vasylyev, M.O. Iefimov: Mater. Sci. Eng. A 458 (2007) 253–261. DOI:10.1016/j.msea.2006.12.049

[20] S. Pour-Ali, A.-R. Kiani-Rashid, A. Babakhani, A. Davoodi: Appl. Surf. Sci. 376 (2016) 121–132. DOI:10.1016/j.apsusc.2016.03.131

[21] Y. Todaka, M. Umemoto, S. Tanaka, K. Tsuchiya: Mater. Trans. 45 (2004) 2209–2213. DOI:10.2320/matertrans.45.2209

[22] I. Altenberger, E.A. Stach, G. Liu, R.K. Nalla, R.O. Ritchie: Scr. Mater. 48 (2003) 1593–1598. DOI:10.1016/S1359-6462(03)00143-X

[23] S. Bagherifard, I. Fernandez-Pariente, R. Ghelichi, M. Guagliano: Int. J. Fatigue. 65 (2014) 64–70. DOI:10.1016/j.ijfatigue.2013.08.022

[24] K.S. Raja, S.A. Namjoshi, M. Misra: Mater. Lett. 59 (2005) 570–574. DOI:10.1016/j.matlet.2004.10.047

[25] G. Ma, B. Xu, H. Wang, H. Si, D. Yang: Mater. Lett. 65 (2011) 1268–1271. DOI:10.1016/j.matlet.2011.01.041

[26] S.M. Hassani-Gangaraj, K.S. Cho, H.-J.L. Voigt, M. Guagliano, C.A. Schuh: Acta Mater. 97 (2015) 105–115. DOI:10.1016/j.actamat.2015.06.054

[27] L. Wagner: Shot peening, John Wiley & Sons, 2003. DOI:10.1002/3527606580

[28] S.M. Hassani-Gangaraj, A. Moridi, M. Guagliano: in: IOP Conf. Ser. Mater. Sci. Eng., IOP Publishing, 2014: p. 12038. DOI:10.1088/1757-899X/63/1/012038

[29] S. Pour-Ali, A.-R. Kiani-Rashid, A. Babakhani, S. Virtanen, M. Allieta: Surf. Coat. Technol. (In press). DOI:10.1016/j.surfcoat.2017.11.062

[30] Y. Todaka, M. Umemoto, K. Tsuchiya: Mater. Trans. 45 (2004) 376–379. DOI:10.2320/matertrans.45.376

[31] R. Fathallah, A. Laamouri, H. Sidhom, C. Braham: Int. J. Fatigue. 26 (2004) 1053–1067. DOI:10.1016/j.ijfatigue.2004.03.007

[32] G.I. Mylonas, G. Labeas: Surf. Coat. Technol. 205 (2011) 4480–4494. DOI:10.1016/j.surfcoat.2011.03.080

[33] S. Bagherifard, R. Ghelichi, M. Guagliano: Appl. Surf. Sci. 259 (2012) 186–194. DOI:10.1016/j.apsusc.2012.07.017

[34] E.J. Mittemeijer, U. Welzel: Modern diffraction methods, John Wiley & Sons, 2013. PMid:23600364

[35] E.J. Mittemeijer, U. Welzel: Zeitschrift Für Krist. Int. J. Struct. Phys. Chem. Asp. Cryst. Mater. 223 (2008) 552–560. DOI:10.1524/zkri.2008.1213

[36] A.C. Larson: R.B. V Dreele, Los Alamos National Laboratory Report No. LAUR, 2004, vol. 86, CrystEngComm. (n.d.) 748.

[37] EN ISO 4287, (1998) 1–65.

[38] S.M. Hassani-Gangaraj, A. Moridi, M. Guagliano, A. Ghidini: Mater. Des. 55 (2014) 492–498. DOI:10.1016/j.matdes.2013.10.015

[39] H.Y. Miao, S. Larose, C. Perron, M. Lévesque: Adv. Eng. Softw. 40 (2009) 1023–1038. DOI:10.1016/j.advengsoft.2009.03.013

[40] K. Dai, J. Villegas, Z. Stone, L. Shaw: Acta Mater. 52 (2004) 5771–5782. DOI:10.1016/j.actamat.2004.08.031

[41] B. Wu, J. Zhang, L. Zhang, Y.-S. Pyoun, R. Murakami: Appl. Surf. Sci. 321 (2014) 318–330. DOI:10.1016/j.apsusc.2014.09.068

[42] G. Liu, J. Lu, K. Lu: Mater. Sci. Eng. A 286 (2000) 91–95. DOI:10.1016/S0921-5093(00)00686-9

[43] X.H. Chen, J. Lu, L. Lu, K. Lu: Scr. Mater. 52 (2005) 1039–1044. DOI:10.1016/j.scriptamat.2005.01.023

[44] B.N. Mordyuk, Y.V. Milman, M.O. Iefimov, G.I. Prokopenko, V.V Silberschmidt, M.I. Danylenko, A. V Kotko: Surf. Coatings Technol. 202 (2008) 4875–4883. DOI:10.1016/j.surfcoat.2008.04.080

[45] M.A. Vasylyev, B.N. Mordyuk, S.I. Sidorenko, S.M. Voloshko, A.P. Burmak: Surf. Coatings Technol. (2017). DOI:10.1016/j.surfcoat.2017.11.019

[46] A. Ghasemi, S.M. Hassani-Gangaraj, A.H. Mahmoudi, G.H. Farrahi, M. Guagliano: Surf. Eng. 32 (2016) 861–870. DOI:10.1080/02670844.2016.1192336

[47] R.E. Schramm, R.P. Reed: Metall. Trans. A 6 (1975) 1345. DOI:10.1007/BF02641927

Correspondence address

Professor Ali-Reza Kiani-Rashid
Materials and Metallurgical Engineering Department
Faculty of Engineering
Ferdowsi University of Mashhad
Azadi Sq.
Mashhad 91775-1111
Iran
Tel.: +98 513 8817182
Fax: +98 513 8807182
E-mail: kianirashid@um.ac.ir
Web: http://kianirashid.profcms.um.ac.ir/

Int. J. Mater. Res. (formerly Z. Metallkd.) 109 (2018) 5

459